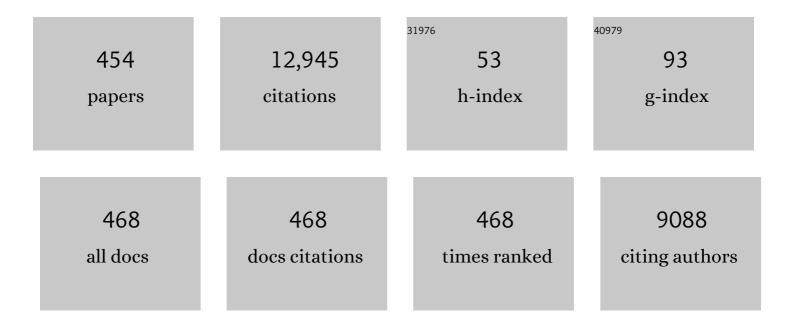
List of Publications by Year in descending order

Source: https://exaly.com/author-pdf/8416184/publications.pdf Version: 2024-02-01



#	Article	IF	CITATIONS
1	3-D Observation with Synchrotron Radiation X-ray CT. Materia Japan, 2022, 61, 65-71.	0.1	0
2	Initiation and propagation of small fatigue crack in beta titanium alloy observed through synchrotron radiation multiscale computed tomography. Engineering Fracture Mechanics, 2022, 263, 108308.	4.3	10
3	Three-dimensional microstructure and mineralogy of a cosmic symplectite in the Acfer 094 carbonaceous chondrite: Implication for its origin. Geochimica Et Cosmochimica Acta, 2022, 323, 220-241.	3.9	5
4	Preliminary analysis of the Hayabusa2 samples returned from C-type asteroid Ryugu. Nature Astronomy, 2022, 6, 214-220.	10.1	136
5	Oxysterol Compounds in Mouse Mutant αA- and αB-Crystallin Lenses Can Improve the Optical Properties of the Lens. , 2022, 63, 15.		8
6	Morphology of Palaeospondylus shows affinity to tetrapod ancestors. Nature, 2022, 606, 109-112.	27.8	4
7	Improved in-vivo airway gene transfer via magnetic-guidance, with protocol development informed by synchrotron imaging. Scientific Reports, 2022, 12, .	3.3	1
8	Detection of small internal fatigue cracks in Tiâ€6Alâ€4V via synchrotron radiation nanocomputed tomography. Fatigue and Fracture of Engineering Materials and Structures, 2022, 45, 2693-2702.	3.4	8
9	Double-multilayer monochromators for high-energy and large-field X-ray imaging applications with intense pink beams at SPring-8 BL20B2. Journal of Synchrotron Radiation, 2022, 29, 1265-1272.	2.4	7
10	Structural diverseness of neurons between brain areas and between cases. Translational Psychiatry, 2021, 11, 49.	4.8	6
11	Tomographic reconstruction using tilted Laue analyser-based X-ray phase-contrast imaging. Journal of Synchrotron Radiation, 2021, 28, 283-291.	2.4	0
12	High-energy x-ray nanotomography introducing an apodization Fresnel zone plate objective lens. Review of Scientific Instruments, 2021, 92, 023701.	1.3	25
13	In situ observation of solidification crack propagation for type 310S and 316L stainless steels during TIG welding using synchrotron X-ray imaging. Journal of Materials Science, 2021, 56, 10653-10663.	3.7	12
14	Microstructural evolution of electrodes in sintering of multi-layer ceramic capacitors (MLCC) observed by synchrotron X-ray nano-CT. Acta Materialia, 2021, 206, 116605.	7.9	30
15	Discovery of primitive CO ₂ -bearing fluid in an aqueously altered carbonaceous chondrite. Science Advances, 2021, 7, .	10.3	16
16	Electrical Conductivity in Texturally Equilibrated Fluidâ€Bearing Forsterite Aggregates at 800°C and 1ÂGPa: Implications for the High Electrical Conductivity Anomalies in Mantle Wedges. Journal of Geophysical Research: Solid Earth, 2021, 126, e2020JB021343.	3.4	13
17	Three-dimensional structural measurement and material identification of an all-solid-state lithium-ion battery by X-Ray nanotomography and deep learning. Journal of Power Sources Advances, 2021, 8, 100048.	5.1	14
18	Assessment of Hydrogen Accumulation Behavior in Al–Zn–Mg Alloy under Strain with Kelvin Force Microscopy. Materials Transactions, 2021, 62, 636-641.	1.2	0

#	Article	IF	CITATIONS
19	Characterization of the Multicellular Membraneâ€Bearing Algae From the Kuanchuanpu Biota (Cambrian: Terreneuvian). Journal of Geophysical Research G: Biogeosciences, 2021, 126, e2020JG006102.	3.0	2
20	Brain capillary structures of schizophrenia cases and controls show a correlation with their neuron structures. Scientific Reports, 2021, 11, 11768.	3.3	15
21	Visualization of Arabidopsis root system architecture in 3D by refraction-contrast X-ray micro-computed tomography. Microscopy (Oxford, England), 2021, 70, 536-544.	1.5	7
22	Mineralogy of fine-grained matrix, fine-grained rim, chondrule rim, and altered mesostasis of a chondrule in Asuka 12169, one of the least altered CM chondrites. Polar Science, 2021, 29, 100727.	1.2	7
23	Development of the Pectoral Lobed Fin in the Australian Lungfish Neoceratodus forsteri. Frontiers in Ecology and Evolution, 2021, 9, .	2.2	2
24	Fracture behavior of thermally aged Ag–Cu composite sinter joint through microscale tensile test coupled with nano X-ray computed tomography. Materials and Design, 2021, 206, 109818.	7.0	9
25	High-Resolution Mapping of Local Photoluminescence Properties in CuO/Cu2O Semiconductor Bi-Layers by Using Synchrotron Radiation. Materials, 2021, 14, 5570.	2.9	1
26	Bone tissue histology of the Early Cretaceous bird <i>Yanornis</i> : evidence for a diphyletic origin of modern avian growth strategies within Ornithuromorpha. Historical Biology, 2020, 32, 1422-1434.	1.4	14
27	In vivo monitoring of bone microstructure by propagation-based phase-contrast computed tomography using monochromatic synchrotron light. Laboratory Investigation, 2020, 100, 72-83.	3.7	4
28	A Modeling Approach for Investigating Opto-Mechanical Relationships in the Human Eye Lens. IEEE Transactions on Biomedical Engineering, 2020, 67, 999-1006.	4.2	12
29	Local Deformation and Fracture Behavior of High-Strength Aluminum Alloys Under Hydrogen Influence. Metallurgical and Materials Transactions A: Physical Metallurgy and Materials Science, 2020, 51, 1-19.	2.2	15
30	An experimental system for time-resolved x-ray diffraction of deforming silicate melt at high temperature. Review of Scientific Instruments, 2020, 91, 095113.	1.3	7
31	Direct observations of nucleant TiB2 particles in cast aluminum by synchrotron radiation multiscale tomography. Materialia, 2020, 10, 100663.	2.7	7
32	An intermediate type of medusa from the early Cambrian Kuanchuanpu Formation, South China. Palaeontology, 2020, 63, 775-789.	2.2	9
33	Cell compaction is not required for the development of gradient refractive index profiles in the embryonic chick lens. Experimental Eye Research, 2020, 197, 108112.	2.6	7
34	Development of a sample holder for synchrotron radiation-based computed tomography and diffraction analysis of extraterrestrial materials. Review of Scientific Instruments, 2020, 91, 035107.	1.3	8
35	The effects of possible contamination by sample holders on samples to be returned by Hayabusa2. Meteoritics and Planetary Science, 2020, 55, 1665-1680.	1.6	6
36	Time-resolved X-ray imaging of solidification cracking for Al-Cu alloy at the weld crater. Materials Characterization, 2020, 167, 110469.	4.4	13

#	Article	IF	CITATIONS
37	Optical development in the zebrafish eye lens. FASEB Journal, 2020, 34, 5552-5562.	0.5	15
38	Damage micromechanisms in high Mn and Zn content 7XXX aluminum alloys. Materials Science & Engineering A: Structural Materials: Properties, Microstructure and Processing, 2020, 793, 139423.	5.6	14
39	Methods for dynamic synchrotron X-ray respiratory imaging in live animals. Journal of Synchrotron Radiation, 2020, 27, 164-175.	2.4	22
40	The universal sample holders of microanalytical instruments of FIB, TEM, NanoSIMS, and STXM-NEXAFS for the coordinated analysis of extraterrestrial materials. Earth, Planets and Space, 2020, 72, .	2.5	16
41	Photon-counting, energy-resolving and super-resolution phase contrast X-ray imaging using an integrating detector Optics Express, 2020, 28, 7080.	3.4	12
42	Development of an X-ray imaging detector for high-energy X-ray microtomography. Journal of Synchrotron Radiation, 2020, 27, 934-940.	2.4	7
43	Emphysema quantified: mapping regional airway dimensions using 2D phase contrast X-ray imaging. Biomedical Optics Express, 2020, 11, 4176.	2.9	7
44	High-Energy X-ray Activities at SPring-8. Synchrotron Radiation News, 2020, 33, 37-43.	0.8	1
45	Assessment of 3D Short Crack Closure in Ti-6Al-4V Alloy Utilizing Synchrotron X-ray Microtomography. MATEC Web of Conferences, 2020, 321, 11051.	0.2	0
46	A Surrogate Approach to Reveal Microstructural Mechanisms Controlling the 3D Short Crack Growth in a Ti-6Al-4V Alloy. MATEC Web of Conferences, 2020, 321, 11004.	0.2	0
47	Pressure and Composition Effects on Sound Velocity and Density of Coreâ€Forming Liquids: Implication to Core Compositions of Terrestrial Planets. Journal of Geophysical Research E: Planets, 2019, 124, 2272-2293.	3.6	39
48	Localized Photoluminescence Imaging of Bi-Layered Cuprous/Cupric Oxide Semiconductor Films by Synchrotron Radiation (Phys. Status Solidi B 3/2019). Physica Status Solidi (B): Basic Research, 2019, 256, 1970018.	1.5	0
49	Assessment of hydrogen embrittlement via image-based techniques in Al–Zn–Mg–Cu aluminum alloys. Acta Materialia, 2019, 176, 96-108.	7.9	63
50	Dendrite fragmentation induced by massive-like δ–γ transformation in Fe–C alloys. Nature Communications, 2019, 10, 3183.	12.8	65
51	Origin of ecdysis: fossil evidence from 535-million-year-old scalidophoran worms. Proceedings of the Royal Society B: Biological Sciences, 2019, 286, 20190791.	2.6	18
52	Initiation and growth behaviour of small internal fatigue cracks in Tiâ€6Alâ€4V via synchrotron radiation microcomputed tomography. Fatigue and Fracture of Engineering Materials and Structures, 2019, 42, 2093-2105.	3.4	38
53	Influence of hydrogen on stress corrosion cracking behavior in Al–10Mg alloy. Keikinzoku/Journal of Japan Institute of Light Metals, 2019, 69, 223-227.	0.4	0
54	Nanometer-Scale Structures of Neurons Differ Between Individuals and Those Differences Become Extraordinary in Schizophrenia. Microscopy and Microanalysis, 2019, 25, 1344-1345.	0.4	0

#	Article	IF	CITATIONS
55	Effects of 3D microstructural distribution on short crack growth behavior in two bimodal Ti–6Al–4V alloys. Materials Science & Engineering A: Structural Materials: Properties, Microstructure and Processing, 2019, 766, 138264.	5.6	8
56	3D multiscale-imaging of processing-induced defects formed during sintering of hierarchical powder packings. Scientific Reports, 2019, 9, 11595.	3.3	27
57	Effect of Cumulative Surface on Pore Development in Chalk. Water Resources Research, 2019, 55, 4801-4819.	4.2	2
58	Defect Structure and Photovoltaic Characteristics of Internally Stacked CuO/Cu ₂ O Photoactive Layer Prepared by Electrodeposition and Heating. ACS Applied Energy Materials, 2019, 2, 4833-4840.	5.1	18
59	Hydrogen partitioning behavior and related hydrogen embrittlement in Al-Zn-Mg alloys. Engineering Fracture Mechanics, 2019, 216, 106503.	4.3	23
60	Optimization of Mechanical Properties in Aluminum Alloys <i>via</i> Hydrogen Partitioning Control. Tetsu-To-Hagane/Journal of the Iron and Steel Institute of Japan, 2019, 105, 240-253.	0.4	0
61	Hydrogen desorption behavior in Al–8%Zn–1%Mg alloy. Keikinzoku/Journal of Japan Institute of Light Metals, 2019, 69, 186-193.	0.4	2
62	Significant contribution of subseafloor microparticles to the global manganese budget. Nature Communications, 2019, 10, 400.	12.8	22
63	Use of ionic liquid for X-ray micro-CT specimen preparation of imbibed seeds. Microscopy (Oxford,) Tj ETQq1 1	0.784314 r 1.5	gBŢ /Overloc
64	Assessment of predominant microstructural features controlling 3D short crack growth behavior via a surrogate approach in Ti-6Al-4V. Materials Science & Engineering A: Structural Materials: Properties, Microstructure and Processing, 2019, 751, 351-362.	5.6	7
65	Three-dimensional alteration of neurites in schizophrenia. Translational Psychiatry, 2019, 9, 85.	4.8	28
66	Discovery of fossil asteroidal ice in primitive meteorite Acfer 094. Science Advances, 2019, 5, eaax5078.	10.3	33
67	Sound velocity and density of liquid Ni68S32 under pressure using ultrasonic and X-ray absorption with tomography methods. Comptes Rendus - Geoscience, 2019, 351, 163-170.	1.2	2
68	The disuse effect on canal network structure and oxygen supply in the cortical bones of rats. Biomechanics and Modeling in Mechanobiology, 2019, 18, 375-385.	2.8	3
69	Localized Photoluminescence Imaging of Biâ€Layered Cuprous/Cupric Oxide Semiconductor Films by Synchrotron Radiation. Physica Status Solidi (B): Basic Research, 2019, 256, 1800119.	1.5	3
70	Synchrotron radiation microtomography of brain hemisphere and spinal cord of a mouse model of multiple sclerosis revealed a correlation between capillary dilation and clinical score. Journal of Comparative Neurology, 2019, 527, 2091-2100.	1.6	1
71	Forearm bone histology of the small theropod <i>Daliansaurus liaoningensis</i> (Paraves:) Tj ETQq1 1 0.78431	.4 rgBT /Ove	erlock 10 Tf 5
72	Contributions of shape and stiffness to accommodative loss in the ageing human lens: a finite element model assessment. Journal of the Optical Society of America A: Optics and Image Science, and Vision, 2019, 36, B116.	1.5	6

#	Article	IF	CITATIONS
73	Development of an X-ray imaging detector to resolve 200  nm line-and-space patterns by using transparent ceramics layers bonded by solid-state diffusion. Optics Letters, 2019, 44, 1403.	3.3	31
74	Age-related changes in eye lens biomechanics, morphology, refractive index and transparency. Aging, 2019, 11, 12497-12531.	3.1	44
75	Evaluation of Macroscopic Mechanical Properties from 3-D Visualization of Microstructure in Sintering. Funtai Oyobi Fummatsu Yakin/Journal of the Japan Society of Powder and Powder Metallurgy, 2019, 66, 604-610.	0.2	0
76	Influence of petrographic textures on the shapes of impact experiment fine fragments measuring several tens of microns: Comparison with Itokawa regolith particles. Icarus, 2018, 302, 109-125.	2.5	17
77	Synchrotron X-ray diffraction characterization of the inheritance of GaN homoepitaxial thin films grown on selective growth substrates. CrystEngComm, 2018, 20, 2861-2867.	2.6	8
78	Method for estimating modulation transfer function from sample images. Micron, 2018, 105, 64-69.	2.2	16
79	Anvil design for slip-free high pressure deformation experiments in a rotational diamond anvil cell. High Pressure Research, 2018, 38, 23-31.	1.2	8
80	PB-05Observation of Arabidopsis Roots Using X-ray Micro Computed Tomography. Microscopy (Oxford,) Tj ETG	Qq0 0.0 rgB	T / gverlock 1
81	PB-06Three-dimensional Morphological Analysis of Supporting Tissues in the Dried Peduncle of Arabidopsis by X-ray Micro-CT. Microscopy (Oxford, England), 2018, 67, i34-i34.	1.5	1
82	Spatial Resolution of Pre-reconstruction Raw Images and their Nano-CT Slices. Microscopy and Microanalysis, 2018, 24, 360-361.	0.4	0
83	Evolution Behavior of Hydrogen-Induced Nano Voids in Al–Zn–Mg–Cu Aluminum Alloys under Loading. Materials Transactions, 2018, 59, 1532-1535.	1.2	6
84	Nondestructive Multiscale X-Ray Tomography by Combining Microtomography and High-Energy Phase-Contrast Nanotomography. Microscopy and Microanalysis, 2018, 24, 108-109.	0.4	26
85	Synchrotron Radiation Nanotomography of Biological Soft Tissues. Microscopy and Microanalysis, 2018, 24, 362-363.	0.4	1
86	Short crack growth behavior and its transitional interaction with 3D microstructure in Ti-6Al-4V. Materials Science & Engineering A: Structural Materials: Properties, Microstructure and Processing, 2018, 738, 229-237.	5.6	14
87	Impacts of Diabetes and an SGLT2 Inhibitor on the Glomerular Number and Volume in db/db Mice, as Estimated by Synchrotron Radiation Micro-CT at SPring-8. EBioMedicine, 2018, 36, 329-346.	6.1	25
88	Observation of Morphology Changes of Fine Eutectic Si Phase in Al-10%Si Cast Alloy during Heat Treatment by Synchrotron Radiation Nanotomography. Materials, 2018, 11, 1308.	2.9	12

89	Improvement of Scanning Procedure for 4D-X-ray Phase Tomography. Microscopy and Microanalysis, 2018, 24, 132-133.	0.4	0
90	The Role of Hydrogen on the Local Fracture Toughness Properties of 7XXX Aluminum Alloys. Metallurgical and Materials Transactions A: Physical Metallurgy and Materials Science, 2018, 49,	2.2	6

Metallurgical and Materials Transactions A: Physical Metallurgy and Materials Science, 2018, 49, 5368-5381. 90 2.2

#	Article	IF	CITATIONS
91	In situ phase contrast X-ray brain CT. Scientific Reports, 2018, 8, 11412.	3.3	39
92	X-Ray Imaging of Formation and Growth of Spheroidal Graphite in Ductile Cast Iron. Materials Science Forum, 2018, 925, 104-109.	0.3	5
93	Influence of hydrogen on strain localization and fracture behavior in Al Zn Mg Cu aluminum alloys. Acta Materialia, 2018, 159, 332-343.	7.9	55
94	Transitional effect of 3D microstructural features on short crack growth behavior in Ti-6Al-4V alloy. The Proceedings of the Materials and Mechanics Conference, 2018, 2018, OS0110.	0.0	0
95	Damage micromechanisms in dual-phase steel investigated with combined phase- and absorption-contrast tomography. Acta Materialia, 2017, 126, 401-412.	7.9	50
96	A <i>Cloudina</i> -like fossil with evidence of asexual reproduction from the lowest Cambrian, South China. Geological Magazine, 2017, 154, 1294-1305.	1.5	20
97	Euendoliths versus ambient inclusion trails from Early Cambrian Kuanchuanpu Formation, South China. Palaeogeography, Palaeoclimatology, Palaeoecology, 2017, 476, 147-157.	2.3	14
98	High-pressure rotational deformation apparatus to 135 GPa. Review of Scientific Instruments, 2017, 88, 044501.	1.3	25
99	Fresnel zone plate with apodized aperture for hard X-ray Gaussian beam optics. Journal of Synchrotron Radiation, 2017, 24, 586-594.	2.4	14
100	In-Situ Monitoring via Synchrotron Radiation Laminography of Thermal Fatigue Cracks at Die-Attached Joints Under Cyclic Energization Loading. , 2017, , .		1
101	Anatomy and affinities of a new 535â€millionâ€yearâ€old medusozoan from the Kuanchuanpu Formation, South China. Palaeontology, 2017, 60, 853-867.	2.2	17
102	Introducing high efficiency image detector to X-ray imaging tomography. Journal of Physics: Conference Series, 2017, 849, 012051.	0.4	9
103	Current status of X-ray phase imaging at SPring-8: Toward 4D X-ray phase tomography for biological samples. Journal of Physics: Conference Series, 2017, 849, 012054.	0.4	1
104	Reconstruction of the multielement apparatus of the earliest Triassic conodont, <i>Hindeodus parvus</i> , using synchrotron radiation X-ray micro-tomography. Journal of Paleontology, 2017, 91, 1220-1227.	0.8	17
105	Influence of intermetallic particles on the initiation and growth behavior of hydrogen micropores during high-temperature exposure in Al-Zn-Mg-Cu aluminum alloys. Scripta Materialia, 2017, 135, 19-23.	5.2	21
106	Advancement of magma fragmentation by inhomogeneous bubble distribution. Scientific Reports, 2017, 7, 16755.	3.3	10
107	CT dose reduction factors in the thousands using X-ray phase contrast. Scientific Reports, 2017, 7, 15953.	3.3	88
108	Electrochemically Grown ZnO Vertical Nanowire Scintillator with Lightâ€Guiding Effect. Physica Status Solidi (A) Applications and Materials Science, 2017, 214, 1700285.	1.8	8

#	Article	IF	CITATIONS
109	High-energy, high-resolution x-ray imaging for metallic cultural heritages. AIP Advances, 2017, 7, .	1.3	7
110	Metasomatic PGE mobilization by carbonatitic melt in the mantle: Evidence from sub-ι⁄4m-scale sulfide–carbonaceous glass inclusion in Tahitian harzburgite xenolith. Chemical Geology, 2017, 475, 87-104.	3.3	14
111	Rheology of basaltic ash from Stromboli volcano inferred from intermittent compression experiments. Journal of Volcanology and Geothermal Research, 2017, 343, 211-219.	2.1	2
112	Investigation of three-dimensional morphology changes of the eutectic Si particles affected by trace P and Sr in Al-7%Si cast alloys by means of synchrotron nano-tomography. Materials Characterization, 2017, 130, 237-242.	4.4	12
113	Three-dimensional study by synchrotron radiation computed tomography of melt distribution in samples doped to enhance contrast. Mineralogical Magazine, 2017, 81, 1203-1222.	1.4	1
114	Observation of the initial process of internal fracture in very high cycle fatigue in Ti-6Al-4V by synchrotron radiation μCT imaging. Transactions of the JSME (in Japanese), 2017, 83, 17-00104-17-00104.	0.2	2
115	Estimating the resolution of real images. Journal of Physics: Conference Series, 2017, 849, 012042.	0.4	1
116	Improvement of quantitative performance of imaging x-ray microscope by reduction of edge-enhancement effect. Journal of Physics: Conference Series, 2017, 849, 012055.	0.4	5
117	Non-Destructive Measurement of Internal Small Fatigue Crack Growth Rate in Ti-6Al-4V. Zairyo/Journal of the Society of Materials Science, Japan, 2017, 66, 928-934.	0.2	5
118	Development of high energy micro-tomography system at SPring-8. , 2017, , .		2
119	Three-dimensional Observation of Nonmetallic Inclusion Clusters in Solid Metal by X-ray Micro-CT. ISIJ International, 2016, 56, 1989-1995.	1.4	13
120	Progress of projection computed tomography by upgrading of the beamline 37XU of SPring-8. AIP Conference Proceedings, 2016, , .	0.4	1
121	3D Fracture Behaviours in Dual-phase Stainless Steel. ISIJ International, 2016, 56, 883-892.	1.4	16
122	SPring-8 BL36XU: Catalytic Reaction Dynamics for Fuel Cells. Journal of Physics: Conference Series, 2016, 712, 012142.	0.4	22
123	Imaging properties and its improvements of scanning/imaging x-ray microscope. AIP Conference Proceedings, 2016, , .	0.4	0
124	Development of sealed sample containers and high resolution micro-tomography. AIP Conference Proceedings, 2016, , .	0.4	2
125	Imaging lung tissue oscillations using high-speed X-ray velocimetry. Journal of Synchrotron Radiation, 2016, 23, 324-330.	2.4	7
126	Detection of small internal fatigue cracks in Ti-6Al-4V by using synchrotron radiation μCT imaging. Mechanical Engineering Letters, 2016, 2, 16-00233-16-00233.	0.6	14

#	Article	IF	CITATIONS
127	PB-03Folded structure of cell surface in dry seeds: real or artifact?. Microscopy (Oxford, England), 2016, 65, i25.1-i25.	1.5	0
128	4D x-ray phase contrast tomography for repeatable motion of biological samples. Review of Scientific Instruments, 2016, 87, 093705.	1.3	14
129	Three-dimensional X-ray visualization of axonal tracts in mouse brain hemisphere. Scientific Reports, 2016, 6, 35061.	3.3	15
130	Note: High-pressure in situ x-ray laminography using diamond anvil cell. Review of Scientific Instruments, 2016, 87, 046105.	1.3	9
131	Optimizing lung aeration at birth using a sustained inflation and positive pressure ventilation in preterm rabbits. Pediatric Research, 2016, 80, 85-91.	2.3	23
132	State of 3-D micro-damage in hydrogen redistributed regions of precharged high strength aluminium alloy. Corrosion Science, 2016, 111, 26-38.	6.6	8
133	Influences of Hydrogen Micropores and Intermetallic Particles on Fracture Behaviors of Al-Zn-Mg-Cu Aluminum Alloys. Metallurgical and Materials Transactions A: Physical Metallurgy and Materials Science, 2016, 47, 6077-6089.	2.2	24
134	Direct observation of grain rotations during coarsening of a semisolid Al–Cu alloy. Proceedings of the United States of America, 2016, 113, E5998-E6006.	7.1	38
135	Quantitative tomography of hydrogen precharged and uncharged Al-Zn-Mg-Cu alloy after tensile fracture. Materials Science & Engineering A: Structural Materials: Properties, Microstructure and Processing, 2016, 670, 300-313.	5.6	12
136	Non-destructive observation of internal fatigue crack growth in Ti–6Al–4V by using synchrotron radiation μCT imaging. International Journal of Fatigue, 2016, 93, 397-405.	5.7	64
137	Three-dimensional structure of brain tissue at submicrometer resolution. AIP Conference Proceedings, 2016, , .	0.4	2
138	Performance of ASTRO-H hard x-ray telescope (HXT). , 2016, , .		5
139	Development of micro-tomography system for materials science at SPring-8. , 2016, , .		3
140	Recent progress of hard x-ray imaging microscopy and microtomography at BL37XU of SPring-8. AIP Conference Proceedings, 2016, , .	0.4	10
141	Nanomorphology of Itokawa regolith particles: Application to space-weathering processes affecting the Itokawa asteroid. Geochimica Et Cosmochimica Acta, 2016, 187, 195-217.	3.9	27
142	Combined FIB microsampling and X-ray microtomography: a powerful tool for the study of tiny fluid inclusions. European Journal of Mineralogy, 2016, 28, 245-256.	1.3	9
143	Divergent evolution of medusozoan symmetric patterns: Evidence from the microanatomy of Cambrian tetramerous cubozoans from South China. Gondwana Research, 2016, 31, 150-163.	6.0	28
144	A method for estimating spatial resolution of real image in the Fourier domain. Journal of Microscopy, 2016, 261, 57-66.	1.8	45

#	Article	IF	CITATIONS
145	Diffraction-amalgamated grain boundary tracking for mapping 3D crystallographic orientation and strain fields during plastic deformation. Acta Materialia, 2016, 107, 310-324.	7.9	29
146	Studies of print-through and reflectivity of x-ray mirrors using thin carbon-fiber-reinforced plastic. Journal of Astronomical Telescopes, Instruments, and Systems, 2016, 2, 014002.	1.8	5
147	Influences of hydrogen on deformation and fracture behaviors of high Zn 7XXX aluminum alloys. International Journal of Fracture, 2016, 200, 13-29.	2.2	37
148	Sound velocity and elastic properties of Fe–Ni and Fe–Ni–C liquids at high pressure. Physics and Chemistry of Minerals, 2016, 43, 229-236.	0.8	19
149	Combined microtomography, thermal desorption spectroscopy, X-ray diffraction study of hydrogen trapping behavior in 7XXX aluminum alloys. Materials Science & Engineering A: Structural Materials: Properties, Microstructure and Processing, 2016, 655, 221-228.	5.6	51
150	Ray-tracing simulation and in-orbit performance of the ASTRO-H hard x-ray telescope (HXT). , 2016, , .		1
151	<i>In situ</i> Observation of Dendrite Growth in Sn-Bi Alloys under Ultrasonic Vibration Using Time-resolved X-ray Imaging. Tetsu-To-Hagane/Journal of the Iron and Steel Institute of Japan, 2016, 102, 170-178.	0.4	3
152	Large-Field X-ray Imaging at SPring-8 BL20B2. Synchrotron Radiation News, 2015, 28, 30-35.	0.8	4
153	Rheological transitions in highâ€ŧemperature volcanic fault zones. Journal of Geophysical Research: Solid Earth, 2015, 120, 2974-2987.	3.4	12
154	X-ray Computerized Tomography Observation of the Interfacial Structure of Liquid Marbles. Bulletin of the Chemical Society of Japan, 2015, 88, 84-88.	3.2	13
155	Differential-phase-contrast knife-edge scan method for precise evaluation of X-ray nanobeam. Japanese Journal of Applied Physics, 2015, 54, 092401.	1.5	4
156	Application of Diffraction-Amalgamated Grain Boundary Tracking to Fatigue Crack Propagation Behavior in High Strength Aluminum Alloy. Materials Transactions, 2015, 56, 424-428.	1.2	6
157	In Situ Observation of Void Nucleation and Growth in a Steel using X-ray Tomography. ISIJ International, 2015, 55, 1474-1482.	1.4	15
158	Morphology of Nonmetallic-inclusion Clusters Observed in Molten Metal by X-ray Micro-CT. Tetsu-To-Hagane/Journal of the Iron and Steel Institute of Japan, 2015, 101, 148-157.	0.4	4
159	Particle Coagulation in Molten Metal Based on Three-Dimensional Analysis of Cluster by X-Ray Micro-Computer Tomography (CT). Tetsu-To-Hagane/Journal of the Iron and Steel Institute of Japan, 2015, 101, 158-167.	0.4	2
160	Three-dimensional imaging of plant tissues using X-ray micro-computed tomography. Plant Morphology, 2015, 27, 21-26.	0.1	20
161	Three-Dimensional Neuronal Structure of Human Cerebral Cortex Determined by Synchrotron-Radiation Microtomography. Microscopy and Microanalysis, 2015, 21, 919-920.	0.4	13
162	X-ray Tomographic Microscopy of Drosophila Brain Network and Skeletonized Model Building in the Three-Dimensional Image. Microscopy and Microanalysis, 2015, 21, 917-918.	0.4	0

#	Article	IF	CITATIONS
163	Three-Dimensional Investigation of Void Coalescence in Free-Cutting Steel using X-ray Tomography. ISIJ International, 2015, 55, 1483-1488.	1.4	4
164	Analysis system of submicron particle tracks in the fine-grained nuclear emulsion by a combination of hard x-ray and optical microscopy. Review of Scientific Instruments, 2015, 86, 073701.	1.3	6
165	The eye lens: age-related trends and individual variations in refractive index and shape parameters. Oncotarget, 2015, 6, 30532-30544.	1.8	46
166	Impact of melt convection induced by ultrasonic wave on dendrite growth in Sn–Bi alloys. Materials Letters, 2015, 150, 135-138.	2.6	30
167	C5-P-02Distribution of intercellular spaces in plant seeds during imbibition and germination observed using X-ray micro-CT. Microscopy (Oxford, England), 2015, 64, i139.2-i139.	1.5	1
168	C3-P-033-D cell geometrical analysis of epidermal and cortical cells in hypocotyl-root axes in arabidopsis seeds using X-ray micro-CT. Microscopy (Oxford, England), 2015, 64, i127.2-i127.	1.5	1
169	C2-O-05Non-destructive observation of aerenchyma development in the primary root of rice using X-ray micro-CT. Microscopy (Oxford, England), 2015, 64, i66.2-i66.	1.5	0
170	Investigation of 3D Grain Shape Characteristics of Lunar Soil Retrieved in Apollo 16 Using Image-Based Discrete-Element Modeling. Journal of Aerospace Engineering, 2015, 28, .	1.4	31
171	Numerical simulation of airflow and microparticle deposition in a synchrotron micro-CT-based pulmonary acinus model. Computer Methods in Biomechanics and Biomedical Engineering, 2015, 18, 1427-1435.	1.6	27
172	Structural changes of polymer-coated microgranules and excipients on tableting investigated by microtomography using synchrotron X-ray radiation. International Journal of Pharmaceutics, 2015, 481, 132-139.	5.2	8
173	X-ray phase-contrast computed tomography visualizes the microstructure and degradation profile of implanted biodegradable scaffolds after spinal cord injury. Journal of Synchrotron Radiation, 2015, 22, 136-142.	2.4	21
174	Surface and internal structures of a space-weathered rim of an Itokawa regolith particle. Icarus, 2015, 257, 230-238.	2.5	36
175	Structural mouthpart interaction evolved already in the earliest lineages of insects. Proceedings of the Royal Society B: Biological Sciences, 2015, 282, 20151033.	2.6	16
176	Influence of Mg on Solidification of Hypereutectic Cast Iron: X-ray Radiography Study. Metallurgical and Materials Transactions A: Physical Metallurgy and Materials Science, 2015, 46, 4937-4946.	2.2	28
177	Localization of shear strain and shear band formation induced by deformation in semi-solid Al-Cu alloys. IOP Conference Series: Materials Science and Engineering, 2015, 84, 012078.	0.6	1
178	Development of vertically aligned ZnO-nanowires scintillators for high spatial resolution x-ray imaging. Applied Physics Letters, 2015, 106, .	3.3	26
179	Refractive index degeneration in older lenses: A potential functional correlate to structural changes that underlie cataract formation. Experimental Eye Research, 2015, 140, 19-27.	2.6	8
180	The influence of Ni and Zn additions on microstructure and phase transformations in Sn–0.7Cu/Cu solder joints. Acta Materialia, 2015, 83, 357-371.	7.9	119

#	Article	IF	CITATIONS
181	Nondestructive Observation of Thermal Fatigue Crack Propagation in FBGA and Die Attached Solder Joints by Synchrotron Radiation X-Ray Laminography. , 2015, , .		0
182	Micro Scale Distribution of Nanoparticles Studied with X-ray Near-Field Scattering. Kobunshi Ronbunshu, 2014, 71, 580-585.	0.2	0
183	Selection and constraint underlie irreversibility of tooth loss in cypriniform fishes. Proceedings of the United States of America, 2014, 111, 7707-7712.	7.1	34
184	ASTRO-H Hard X-ray Telescope (HXT). , 2014, , .		5
185	Recent progress in the ground calibration of the ASTRO-H Hard X-ray telescope (HXT-2). , 2014, , .		2
186	Formation behaviour of blister in cast aluminium alloy. International Journal of Cast Metals Research, 2014, 27, 369-377.	1.0	22
187	<i>In Vivo</i> X-Ray Imaging Reveals Improved Airway Surface Hydration after a Therapy Designed for Cystic Fibrosis. American Journal of Respiratory and Critical Care Medicine, 2014, 190, 469-472.	5.6	31
188	Ideal Osmotic Spaces for Chlorobionts or Cyanobionts Are Differentially Realized by Lichenized Fungi Â Â. Plant Physiology, 2014, 166, 337-348.	4.8	9
189	In Situ Observation of Deformation in Semi-solid Fe-C Alloys at High Shear Rate. Metallurgical and Materials Transactions A: Physical Metallurgy and Materials Science, 2014, 45, 5613-5623.	2.2	17
190	The True Origin of Ductile Fracture in Aluminum Alloys. Metallurgical and Materials Transactions A: Physical Metallurgy and Materials Science, 2014, 45, 765-776.	2.2	91
191	Solidification of Sn-0.7Cu-0.15Zn Solder: In Situ Observation. Metallurgical and Materials Transactions A: Physical Metallurgy and Materials Science, 2014, 45, 918-926.	2.2	23
192	Low Core-Mantle Boundary Temperature Inferred from the Solidus of Pyrolite. Science, 2014, 343, 522-525.	12.6	224
193	Development of 3D crystallographic orientation measurement for grain deformation analysis in aluminum alloy. Transactions of Nonferrous Metals Society of China, 2014, 24, 2094-2101.	4.2	0
194	Threeâ€dimensional microstructure of samples recovered from asteroid 25143 Itokawa: Comparison with <scp>LL</scp> 5 and <scp>LL</scp> 6 chondrite particles. Meteoritics and Planetary Science, 2014, 49, 172-187.	1.6	48
195	Optical properties of the lens: An explanation for the zones of discontinuity. Experimental Eye Research, 2014, 124, 93-99.	2.6	23
196	Effects of Stress Triaxiality on Damage Evolution from Pre-Existing Hydrogen Pores in Aluminum Alloy. Materials Transactions, 2014, 55, 383-386.	1.2	3
197	Recent progress of X-ray tomography in material science field. Keikinzoku/Journal of Japan Institute of Light Metals, 2014, 64, 510-517.	0.4	0
198	Image-based finite element analysis for reverse 4D materials engineering: ductile fracture originated from hydrogen pores. Keikinzoku/Journal of Japan Institute of Light Metals, 2014, 64, 611-612.	0.4	1

#	Article	IF	CITATIONS
199	Spatiotemporal development of soaked protein crystal. Scientific Reports, 2014, 4, 5731.	3.3	4
200	Quantitative and dynamic measurements of biologicalÂfresh samples with X-ray phase contrastÂtomography. Journal of Synchrotron Radiation, 2014, 21, 1347-1357.	2.4	24
201	Changes in Positive End-Expiratory Pressure Alter the Distribution of Ventilation within the Lung Immediately after Birth in Newborn Rabbits. PLoS ONE, 2014, 9, e93391.	2.5	23
202	W-Concentration 3D Mapping in SKH51 Steel by Dual-Energy K-Absorption Edge Subtraction Imaging. ISIJ International, 2014, 54, 141-147.	1.4	2
203	Application of Diffraction-Amalgamated Grain Boundary Tracking (DAGT) to Fatigue Crack Propagation Behavior in High Strength Aluminum Alloy. , 2014, , 91-96.		0
204	Internal structure changes of eyelash induced by eye makeup. Journal of Cosmetic Science, 2014, 65, 217-24.	0.1	2
205	Stereological Analysis of Nonspherical Particles in Solid Metal. Metallurgical and Materials Transactions B: Process Metallurgy and Materials Processing Science, 2013, 44, 750-761.	2.1	15
206	Airway distension during lung inflation in healthy and allergic-sensitised mice in vivo. Respiratory Physiology and Neurobiology, 2013, 185, 639-646.	1.6	11
207	Compression and recovery micro-mechanisms in flexible graphite. Carbon, 2013, 59, 184-191.	10.3	15
208	Investigation of internal structure of fine granules by microtomography using synchrotron X-ray radiation. International Journal of Pharmaceutics, 2013, 445, 93-98.	5.2	27
209	Coupled effect of magma degassing and rheology on silicic volcanism. Earth and Planetary Science Letters, 2013, 362, 163-170.	4.4	63
210	Study of creep cavitation behavior in tempered martensitic steel using synchrotron micro-tomography and serial sectioning techniques. Materials Science & Engineering A: Structural Materials: Properties, Microstructure and Processing, 2013, 564, 525-538.	5.6	34
211	Micro-pore development phenomenon in hydrogen pre-charged aluminum alloy studied using synchrotron X-ray micro-tomography. Applied Physics Letters, 2013, 103, .	3.3	10
212	Real time synchrotron X-ray observations of solidification in hypoeutectic Al–Si alloys. Materials Characterization, 2013, 85, 134-140.	4.4	34
213	Visualization of nanoscale deformation in polymer composites with zernike-type phase-contrast X-ray microscopy and the finite element method. Polymer Journal, 2013, 45, 64-69.	2.7	8
214	Characterization of Cell Wall Microstructure and Damage Behavior of Alloyed Aluminum Foam via Synchrotronâ€Based Microtomography. Advanced Engineering Materials, 2013, 15, 149-152.	3.5	3
215	Nondestructive observation of fatigue crack propagation process in some solder joints by synchrotron radiation X-ray micro-tomography. , 2013, , .		0
216	Three-dimensional observation and morphological analysis of organic nanoglobules in a carbonaceous chondrite using X-ray micro-tomography. Geochimica Et Cosmochimica Acta, 2013, 116, 84-95.	3.9	14

#	Article	IF	CITATIONS
217	Grain boundary tracking: A four-dimensional visualization technique for determining grain boundary geometry via local strain mapping. Acta Materialia, 2013, 61, 5535-5548.	7.9	31
218	Analytical dual-energy microtomography: A new method for obtaining three-dimensional mineral phase images and its application to Hayabusa samples. Geochimica Et Cosmochimica Acta, 2013, 116, 5-16.	3.9	55
219	Three-dimensional observation of carbonaceous chondrites by synchrotron radiation X-ray CT – Quantitative analysis and developments for the future sample return missions. Geochimica Et Cosmochimica Acta, 2013, 116, 17-32.	3.9	20
220	Three-dimensional network of Drosophila brain hemisphere. Journal of Structural Biology, 2013, 184, 271-279.	2.8	30
221	Cavitation during high-temperature deformation in Al–Mg alloys. Acta Materialia, 2013, 61, 2403-2413. Acceleration of deposition of <mml:math <="" td="" xmlns:mml="http://www.w3.org/1998/Math/MathML"><td>7.9</td><td>32</td></mml:math>	7.9	32
222	altimg="si0006.gif" overflow="scroll"> <mml:mi mathvariant="normal">A<mml:msub><mml:mrow><mml:mi>Î²</mml:mi></mml:mrow>< peptide on ultrasonically formed <mml:math <br="" xmlns:mml="http://www.w3.org/1998/Math/MathML">altimg="si000".gif" overflow="scroll"><mml:mi< td=""><td>mml:mn> 10.1</td><td>1 10</td></mml:mi<></mml:math></mml:msub></mml:mi 	mml:mn> 10.1	1 10
223	mathvariant="normal">A <mml:msub><mml:mrow><mml:mi>βBioelectro Robust Liquid Marbles Stabilized with Surface-Modified Halloysite Nanotubes. Langmuir, 2013, 29, 14971-14975.</mml:mi></mml:mrow></mml:msub>	3.5	51
224	The role of lung inflation and sodium transport in airway liquid clearance during lung aeration in newborn rabbits. Pediatric Research, 2013, 73, 443-449.	2.3	41
225	Micro-CT observations of the 3D distribution of calcium oxalate crystals in cotyledons during maturation and germination inLotus miyakojimaeseeds. Microscopy (Oxford, England), 2013, 62, 353-361.	1.5	19
226	Nondestructive Three-Dimensional Observation of the Influence of Zirconium Inclusions in Laser-Irradiated Fusion-Spliced Optical Fiber on Core Structure Changes Using Synchrotron Radiation X-ray Micro-Computed Tomography. Japanese Journal of Applied Physics, 2013, 52, 096602.	1.5	2
227	Development of large-field high-resolution hard x-ray imaging microscopy and microtomography with Fresnel zone plate objective. , 2013, , .		7
228	Mechanisms of Ultrasonically Induced Fibrillation of Amyloid β _{1–40} Peptides. Japanese Journal of Applied Physics, 2013, 52, 07HE10.	1.5	10
229	Study of Creep Damage in a 10.86% Cr Heat Resistant Steel using Synchrotron X-Ray Microtomography. Advanced Materials Research, 2013, 794, 476-483.	0.3	0
230	Sagittal focusing of synchrotron radiation X-rays using a winged crystal. Journal of Synchrotron Radiation, 2013, 20, 219-225.	2.4	14
231	X-ray microtomographic visualization of <i>EscherichiaÂcoli</i> by metalloprotein overexpression. Journal of Synchrotron Radiation, 2013, 20, 581-586.	2.4	5
232	X-ray micro-tomography using white beam radiation from SPring-8. Journal of Instrumentation, 2013, 8, P07018-P07018.	1.2	3
233	Three-dimensional phase-contrast X-ray microtomographyÂwith scanning–imaging X-rayÂmicroscope optics. Journal of Synchrotron Radiation, 2013, 20, 793-800.	2.4	14
234	Murine pulmonary acinar mechanics during quasi-static inflation using synchrotron refraction-enhanced computed tomography. Journal of Applied Physiology, 2013, 115, 219-228.	2.5	47

#	Article	IF	CITATIONS
235	Development of Scanning-Imaging X-Ray Microscope for Quantitative Three-Dimensional Phase Contrast Microimaging. Journal of Physics: Conference Series, 2013, 463, 012034.	0.4	1
236	First result from a ground calibration of the Hard X-ray Telescope (HXT) onboard ASTRO-H satellite. Proceedings of SPIE, 2013, , .	0.8	1
237	Hard X-ray Imaging Microscopy using X-ray Guide Tube as Beam Condenser for Field Illumination. Journal of Physics: Conference Series, 2013, 463, 012028.	0.4	9
238	3D/4D fracture mechanics evaluation on shear band of aluminum alloys. Keikinzoku/Journal of Japan Institute of Light Metals, 2013, 63, 188-195.	0.4	1
239	Relationship between resolution and rotation stage in imaging X-ray CT. Keikinzoku/Journal of Japan Institute of Light Metals, 2013, 63, 273-278.	0.4	1
240	Development of X-ray triscopic imaging system towards three-dimensional measurements of dynamical samples. Journal of Instrumentation, 2013, 8, C05002-C05002.	1.2	6
241	Development of 3D Deformation Analysis Method in Polycrystalline Metal by Combining Synchrotron Radiation Tomography with X-Ray Diffraction. Nippon Kinzoku Gakkaishi/Journal of the Japan Institute of Metals, 2013, 77, 375-384.	0.4	1
242	Effects of Hydrogen Micro Pores on Mechanical Properties in A2024 Aluminum Alloys. Materials Transactions, 2013, 54, 2195-2201.	1.2	23
243	Morphology of Nonmetallic-inclusion Clusters Observed in Molten Metal by X-ray Micro-Computed Tomography (CT). ISIJ International, 2013, 53, 1943-1952.	1.4	20
244	Particle Coagulation in Molten Metal Based on Three-Dimensional Analysis of Cluster by X-Ray Micro-Computer Tomography (CT). ISIJ International, 2013, 53, 1958-1967.	1.4	12
245	Application of Synchrotron Radiation X-Ray Laminography to Nondestructive Evaluation of the Fatigue Crack Propagation Process in Flip Chip Solder Joints. , 2013, , .		1
246	Measuring Airway Surface Liquid Depth in Ex Vivo Mouse Airways by X-Ray Imaging for the Assessment of Cystic Fibrosis Airway Therapies. PLoS ONE, 2013, 8, e55822.	2.5	21
247	Real Time Synchrotron X-Ray Imaging for Nucleation and Growth of Cu ₆ Sn ₅ in Sn-7Cu-0.05Ni High Temperature Lead-Free Solder Alloys. Advanced Materials Research, 2012, 626, 200-204.	0.3	6
248	In-situobservation of peritectic solidification in Sn-Cd and Fe-C alloys. IOP Conference Series: Materials Science and Engineering, 2012, 27, 012084.	0.6	25
249	Visualization of neurons in the brain with phase-contrast CT. , 2012, , .		0
250	Extracting tissue and cell outlines of Arabidopsis seeds using refraction contrast X-ray CT at the SPring-8 facility. AIP Conference Proceedings, 2012, , .	0.4	7
251	Single grating x-ray imaging for dynamic biological systems. , 2012, , .		3
252	Optimization of X-ray phase contrast imaging system toward high-sensitivity measurements of biological organs. AIP Conference Proceedings, 2012, , .	0.4	7

#	Article	IF	CITATIONS
253	Demonstration of osmotically dependent promotion of aerenchyma formation at different levels in the primary roots of rice using a â€~sandwich' method and X-ray computed tomography. Annals of Botany, 2012, 110, 503-509.	2.9	39
254	Performance Test and Evaluation of Multilevel Fresnel Zone Plate with Three-Step Profile Fabricated with Electron-Beam Lithography. Japanese Journal of Applied Physics, 2012, 51, 022502.	1.5	8
255	Development of fast and high throughput tomography using CMOS image detector at SPring-8. Proceedings of SPIE, 2012, , .	0.8	36
256	Development of diffraction-amalgamated grain-boundary tracking technique and its application to polycrystalline metals. Proceedings of SPIE, 2012, , .	0.8	0
257	Current status of ASTRO-H Hard X-ray Telescopes (HXTs). , 2012, , .		7
258	Experimental constraints on permeable gas transport in crystalline silicic magmas. Contributions To Mineralogy and Petrology, 2012, 164, 493-504.	3.1	26
259	Massive transformation from <i>δ</i> phase to <i>γ</i> phase in Fe–C alloys and strain induced in solidifying shell. IOP Conference Series: Materials Science and Engineering, 2012, 33, 012036.	0.6	38
260	Microstructure of Multilayer Fresnel Zone Plate for X-ray Focusing. Physics Procedia, 2012, 32, 157-160.	1.2	3
261	4D Visualization of a Cathode Catalyst Layer in a Polymer Electrolyte Fuel Cell by 3D Laminography–XAFS. Angewandte Chemie - International Edition, 2012, 51, 10311-10314.	13.8	63
262	Spatial resolution of synchrotron x-ray microtomography in high energy range: Effect of x-ray energy and sample-to-detector distance. Applied Physics Letters, 2012, 101, .	3.3	22
263	Differential phase contrast x-ray microimaging with scanning-imaging x-ray microscope optics. Review of Scientific Instruments, 2012, 83, 083701.	1.3	4
264	Recent results of hard x-ray characterization of ASTRO-H HXT at SPring-8. Proceedings of SPIE, 2012, , .	0.8	4
265	Imaging and spectral performance of CdTe double-sided strip detectors for the hard x-ray imager onboard ASTRO-H. , 2012, , .		6
266	SIZE AND DENSITY ESTIMATION FROM IMPACT TRACK MORPHOLOGY IN SILICA AEROGEL: APPLICATION TO DUST FROM COMET 81P/WILD 2. Astrophysical Journal, 2012, 744, 18.	4.5	18
267	Synchrotron radiography of direct-shear in semi-solid alloys. IOP Conference Series: Materials Science and Engineering, 2012, 27, 012086.	0.6	9
268	High-resolution Observation of Steel Using X-ray Tomography Technique. ISIJ International, 2012, 52, 516-521.	1.4	25
269	Phase-contrast X-ray microtomography of mouse fetus. Biology Open, 2012, 1, 269-274.	1.2	34
270	Three-dimensional evaluation of the compression and recovery behavior in a flexible graphite sheet by synchrotron radiation microtomography. Materials Characterization, 2012, 69, 52-62.	4.4	21

#	Article	IF	CITATIONS
271	Diffraction-Amalgamated Grain-boundary Tracking (DAGT) technique and its application to an aluminum alloy. , 2012, , 9-14.		4
272	Turbulent Coagulation of Solid Particles in Molten Aluminium—Kinetics of Cluster Formation. , 2012, , 1337-1342.		2
273	Seed-Dependent Deposition Behavior of Al² Peptides Studied with Wireless Quartz-Crystal-Microbalance Biosensor. Analytical Chemistry, 2011, 83, 4982-4988.	6.5	21
274	Optimizing the Illumination in a Hard X-ray Microscope with Integrated Talbot Interferometer. AIP Conference Proceedings, 2011, , .	0.4	3
275	SPring-8 X-Ray Micro-Tomography Observations of Zirconium Inclusions in CO\$_{2}\$ Laser Fusion Splice for Single Mode Optical Fibers. IEEE Transactions on Components, Packaging and Manufacturing Technology, 2011, 1, 100-110.	2.5	1
276	Development of X-ray Imaging for Observing Solidification of Carbon Steels. ISIJ International, 2011, 51, 402-408.	1.4	100
277	Hollow-Cone Illumination for Hard X-ray Imaging Microscopy by Rotating-Grating Condenser Optics. AIP Conference Proceedings, 2011, , .	0.4	6
278	Present Status of the Nanotomography System at BL47XU at SPring-8 and Its Efficiency Improvement Using Double-Condenser Optics. AIP Conference Proceedings, 2011, , .	0.4	13
279	Angular resolution measurements at SPring-8 of a hard x-ray optic for the New Hard X-ray Mission. Proceedings of SPIE, 2011, , .	0.8	4
280	The current status of reflector production and hard x-ray characterization for ASTRO-H/HXT. Proceedings of SPIE, 2011, , .	0.8	0
281	Building Human Brain Network in 3D Coefficient Map Determined by X-ray Microtomography. AlP Conference Proceedings, 2011, , .	0.4	7
282	Simultaneous Measurement of Oxygen Diffusivity and Visualization of Moisture Distribution in Gas Diffusion Layer with Wettability Distribution for Improvement of Polymer Electrolyte Fuel Cell Performance. 880-02 Nihon Kikai Gakkai Ronbunshū Transactions of the Japan Society of Mechanical Engineers Series B B-hen, 2011, 77, 2019-2027.	0.2	2
283	Development of an X-ray Micro-Laminography System at SPring-8. , 2011, , .		14
284	The Effect of Changing Positive End-Expiratory Pressures on the Spatial Pattern of Lung Ventilation in Newborn Rabbits Ventilated from Birth. Pediatric Research, 2011, 70, 45-45.	2.3	0
285	Three Dimensional and Nondestructive Evaluation of Thermal Fatigue Crack Propagation Process in Complex-Shaped Solder Joints by Synchrotron Radiation X-Ray Micro-Tomography. , 2011, , .		2
286	Direct observation of deformation in semi-solid carbon steel. Scripta Materialia, 2011, 64, 1129-1132.	5.2	81
287	Phase contrast image segmentation using a Laue analyser crystal. Physics in Medicine and Biology, 2011, 56, 515-534.	3.0	42
288	Three-Dimensional Cortical Bone Microstructure in a Rat Model of Hypoxia-Induced Growth Retardation. Calcified Tissue International, 2011, 88, 54-62.	3.1	13

#	Article	IF	CITATIONS
289	In Vivo CT Quantification of Trabecular Bone Dynamics in Mice after Sciatic Neurectomy Using Monochromatic Synchrotron Radiation. Calcified Tissue International, 2011, 88, 432-441.	3.1	7
290	Granular deformation mechanisms in semi-solid alloys. Acta Materialia, 2011, 59, 4933-4943.	7.9	89
291	Comparison of lens- and fiber-coupled CCD detectorsÂfor X-ray computed tomography. Journal of Synchrotron Radiation, 2011, 18, 217-223.	2.4	42
292	Development of an X-ray real-time stereo imaging technique using synchrotron radiation. Journal of Synchrotron Radiation, 2011, 18, 569-574.	2.4	26
293	In situ investigation of unidirectional solidification in Sn–0.7Cu and Sn–0.7Cu–0.06Ni. Acta Materialia, 2011, 59, 4043-4054.	7.9	56
294	Statistical assessment of fatigue crack initiation from sub-surface hydrogen micropores in high-quality die-cast aluminum. Acta Materialia, 2011, 59, 4990-4998.	7.9	42
295	Localized deformation during fracture of high-strength aluminum alloy. Procedia Engineering, 2011, 10, 2591-2596.	1.2	4
296	Development of x-ray laminography under an x-ray microscopic condition. Review of Scientific Instruments, 2011, 82, 073706.	1.3	18
297	Three-Dimensional Structure of Hayabusa Samples: Origin and Evolution of Itokawa Regolith. Science, 2011, 333, 1125-1128.	12.6	249
298	Surfactant Increases the Uniformity of Lung Aeration at Birth in Ventilated Preterm Rabbits. Pediatric Research, 2011, 70, 50-55.	2.3	37
299	Combined Lung Imaging and Respiratory Physiology Research at SPring-8. Synchrotron Radiation News, 2011, 24, 19-23.	0.8	3
300	Towards a high-resolution local tomography using statistical iterative reconstruction. , 2011, , .		0
301	Optical Properties of In Situ Eye Lenses Measured with X-Ray Talbot Interferometry: A Novel Measure of Growth Processes. PLoS ONE, 2011, 6, e25140.	2.5	57
302	Current Status of Microtomography with Synchrotron Radiation X-ray Source. Journal of the Vacuum Society of Japan, 2011, 54, 47-55.	0.3	5
303	Current status of hard x-ray characterization of ASTRO-H HXT at SPring-8. , 2010, , .		4
304	A high precision recipe for correcting images distorted by a tapered fiber optic. Journal of Instrumentation, 2010, 5, P09008-P09008.	1.2	7
305	Four-Dimensional Annihilation Behaviors of Micro Pores during Surface Cold Working. Materials Transactions, 2010, 51, 1288-1295.	1.2	29
306	Application of Dual-Energy K-Edge Subtraction Imaging to Assessment of Heat Treatments in Al-Cu Alloys. Materials Transactions, 2010, 51, 2045-2048.	1.2	22

#	Article	IF	CITATIONS
307	Growth behavior of hydrogen micro pores during ductile fracture of a 5154 aluminum alloy. Keikinzoku/Journal of Japan Institute of Light Metals, 2010, 60, 409-410.	0.4	1
308	Measurement of hard X-ray coherence in the presence of a rotating random-phase-screen diffuser. Optics Communications, 2010, 283, 216-225.	2.1	14
309	Submicrometer tomographic resolution examined using a micro-fabricated test object. Micron, 2010, 41, 90-95.	2.2	16
310	Estimation of presampling modulation transfer function in synchrotron radiation microtomography. Nuclear Instruments and Methods in Physics Research, Section A: Accelerators, Spectrometers, Detectors and Associated Equipment, 2010, 621, 615-619.	1.6	15
311	Fabrication and testing of sputtered-sliced kinoform style Fresnel zone plate. Vacuum, 2010, 84, 1457-1459.	3.5	4
312	Influence of high-temperature solution treatments on mechanical properties of an Al–Si–Cu aluminum alloy. Acta Materialia, 2010, 58, 2014-2025.	7.9	64
313	A new technique to examine individual pollutant particle and fibre deposition and transit behaviour in live mouse trachea. Journal of Synchrotron Radiation, 2010, 17, 719-729.	2.4	12
314	Synchrotron Micro-XRF Measurements of Trace Element Distributions in BCA Type Solders and Solder Joints. Transactions of the Japan Institute of Electronics Packaging, 2010, 3, 40-46.	0.4	14
315	Regular Structure Formation of Hypermonotectic Al-In Alloys. Materials Science Forum, 2010, 649, 131-136.	0.3	4
316	Microtomographic Analysis of Neuronal Circuits of Human Brain. Cerebral Cortex, 2010, 20, 1739-1748.	2.9	35
317	Differential Phase-Contrast Scanning X-Ray Microscope For Observation Of Low-Z element Specimen. AIP Conference Proceedings, 2010, , .	0.4	5
318	Development of fast (sub-minute) micro-tomography. AIP Conference Proceedings, 2010, , .	0.4	25
319	Investigation of Imaging Properties of Mouse Eyes Using X-ray Phase Contrast Tomography. AIP Conference Proceedings, 2010, , .	0.4	10
320	Assessment of 3D inhomogeneous microstructure of highly alloyed aluminium foam via dual energy K-edge subtraction imaging. Philosophical Magazine, 2010, 90, 1853-1871.	1.6	9
321	Shear deformation experiments on vesicular rhyolite: Implications for brittle fracturing, degassing, and compaction of magmas in volcanic conduits. Journal of Geophysical Research, 2010, 115, .	3.3	80
322	2D and 3D X-ray phase retrieval of†multi-material objects using a†single defocus distance. Optics Express, 2010, 18, 6423.	3.4	141
323	Assessment of the use of a diffuser in propagation-based x-ray phase contrast imaging. Optics Express, 2010, 18, 13478.	3.4	12
324	X-ray phase, absorption and scatter retrieval using two or more phase contrast images. Optics Express, 2010, 18, 19994.	3.4	33

#	Article	IF	CITATIONS
325	The role of trace element segregation in the eutectic modification of hypoeutectic Al–Si alloys. Journal of Alloys and Compounds, 2010, 489, 415-420.	5.5	132
326	Non-destructive observation of meteorite chips using quantitative analysis of optimized X-ray micro-computed tomography. Earth and Planetary Science Letters, 2010, 299, 359-367.	4.4	23
327	Threeâ€dimensional shapes and Fe contents of Stardust impact tracks: A track formation model and estimation of comet Wild 2 coma dust particle densities. Meteoritics and Planetary Science, 2010, 45, 1302-1319.	1.6	14
328	Development of high pressure apparatus for X-ray microtomography at SPring-8. Journal of Physics: Conference Series, 2010, 215, 012026.	0.4	14
329	3D Shape Characterization and Image-Based DEM Simulation of the Lunar Soil Simulant FJS-1. Journal of Aerospace Engineering, 2009, 22, 15-23.	1.4	141
330	Establishing Functional Residual Capacity at Birth: The Effect of Sustained Inflation and Positive End-Expiratory Pressure in a Preterm Rabbit Model. Pediatric Research, 2009, 65, 537-541.	2.3	178
331	Effect of Sustained Inflation Length on Establishing Functional Residual Capacity at Birth in Ventilated Premature Rabbits. Pediatric Research, 2009, 66, 295-300.	2.3	141
332	Local crack driving force analysis of a fatigue crack by a microstructural tracking method. Scripta Materialia, 2009, 61, 489-492.	5.2	13
333	Sarcoptes scabiei var. hominis: Three-dimensional structure of a female imago and crusted scabies lesions by X-ray micro-CT. Experimental Parasitology, 2009, 122, 268-272.	1.2	7
334	Real-time non-invasive detection of inhalable particulates delivered into live mouse airways. Journal of Synchrotron Radiation, 2009, 16, 553-561.	2.4	17
335	Confocal full-field X-ray microscope for novel three-dimensional X-ray imaging. Journal of Synchrotron Radiation, 2009, 16, 616-621.	2.4	27
336	IMAGING LUNG AERATION AND LUNG LIQUID CLEARANCE AT BIRTH USING PHASE CONTRAST Xâ€RAY IMAGING. Clinical and Experimental Pharmacology and Physiology, 2009, 36, 117-125.	1.9	64
337	The effects of microstructure on creep behaviour—A study through synchrotron X-ray tomography. Materials Science & Engineering A: Structural Materials: Properties, Microstructure and Processing, 2009, 513-514, 222-227.	5.6	11
338	Quasi-blazed type multilayer zone plate for X-rays. Vacuum, 2009, 84, 578-580.	3.5	3
339	Observation of kinoform-style multilayer Fresnel zone plate by scanning ion microscopy. Vacuum, 2009, 84, 669-671.	3.5	3
340	Chain structure in the unidirectionally solidified Al2O3–YAG–ZrO2 eutectic composite. Journal of Crystal Growth, 2009, 311, 3765-3770.	1.5	13
341	Growth behavior of hydrogen micropores in aluminum alloys during high-temperature exposure. Acta Materialia, 2009, 57, 2277-2290.	7.9	150
342	Three-dimensional fatigue crack growth behavior in an aluminum alloy investigated with in situ high-resolution synchrotron X-ray microtomography. Acta Materialia, 2009, 57, 3287-3300.	7.9	63

#	Article	IF	CITATIONS
343	Healing behavior of preexisting hydrogen micropores in aluminum alloys during plastic deformation. Acta Materialia, 2009, 57, 4391-4403.	7.9	93
344	<i>In situ</i> observation of solidification phenomena in Al–Cu and Fe–Si–Al alloys. International Journal of Cast Metals Research, 2009, 22, 15-21.	1.0	81
345	Magma deformation may induce non-explosive volcanism via degassing through bubble networks. Earth and Planetary Science Letters, 2009, 281, 267-274.	4.4	110
346	Threeâ€dimensional structures and elemental distributions of Stardust impact tracks using synchrotron microtomography and Xâ€ray fluorescence analysis. Meteoritics and Planetary Science, 2009, 44, 1203-1224.	1.6	30
347	Zernike phase-contrast x-ray microscope with pseudo-Kohler illumination generated by sectored (polygon) condenser plate. Journal of Physics: Conference Series, 2009, 186, 012020.	0.4	35
348	High-definition high-throughput micro-tomography at SPring-8. Journal of Physics: Conference Series, 2009, 186, 012050.	0.4	12
349	Quasi-kinoform type multilayer zone plate with high diffraction efficiency for high-energy X-rays. Journal of Physics: Conference Series, 2009, 186, 012075.	0.4	13
350	Roles of Pre-Existing Hydrogen Micropores on Ductile Fracture. Materials Transactions, 2009, 50, 2285-2290.	1.2	39
351	Three-dimensional observation of micro-pores in a 2024 aluminum alloy by synchrotron X-ray projection- and imaging-type microtomography techniques. Keikinzoku/Journal of Japan Institute of Light Metals, 2009, 59, 30-34.	0.4	8
352	Inspiration regulates the rate and temporal pattern of lung liquid clearance and lung aeration at birth. Journal of Applied Physiology, 2009, 106, 1888-1895.	2.5	100
353	Current status of the Astro-H X-ray Telescope system. , 2009, , .		3
354	Positive end-expiratory pressure enhances development of a functional residual capacity in preterm rabbits ventilated from birth. Journal of Applied Physiology, 2009, 106, 1487-1493.	2.5	134
355	Element-specific microtomographic imaging of <i>Drosophila</i> brain stained with high- <i>Z</i> probes. Journal of Synchrotron Radiation, 2008, 15, 374-377.	2.4	20
356	<i>In situ</i> observation of water distribution and behaviour in a polymer electrolyte fuel cell by synchrotron X-ray imaging. Journal of Synchrotron Radiation, 2008, 15, 329-334.	2.4	50
357	Evaluation of the improved three-dimensional resolution of a synchrotron radiation computed tomograph using a micro-fabricated test pattern. Journal of Synchrotron Radiation, 2008, 15, 648-654.	2.4	13
358	High-density three-dimensional mapping of internal strain by tracking microstructural features. Acta Materialia, 2008, 56, 2167-2181.	7.9	117
359	Direct measurement procedure for three-dimensional local crack driving force using synchrotron X-ray microtomography. Acta Materialia, 2008, 56, 6027-6039.	7.9	88
360	Multilevel-type multilayer X-ray lens (Fresnel zone plate) by sputter deposition. Vacuum, 2008, 83, 691-694.	3.5	10

#	Article	IF	CITATIONS
361	Development of high-resolution 4D <i>in vivo</i> CT for visualization of cardiac and respiratory deformations of small animals. Physics in Medicine and Biology, 2008, 53, 4285-4301.	3.0	43
362	Highâ€resolution visualization of airspace structures in intact mice via synchrotron phaseâ€contrast Xâ€ray imaging (PCXI). Journal of Anatomy, 2008, 213, 217-227.	1.5	54
363	Three-dimensional microtomographic imaging of human brain cortex. Brain Research, 2008, 1199, 53-61.	2.2	22
364	Bulk mineralogy and threeâ€dimensional structures of individual Stardust particles deduced from synchrotron Xâ€ray diffraction and microtomography analysis. Meteoritics and Planetary Science, 2008, 43, 247-259.	1.6	47
365	Detecting micrometerâ€scale platinumâ€group minerals in mantle peridotite with microbeam synchrotron radiation Xâ€ray fluorescence analysis. Geochemistry, Geophysics, Geosystems, 2008, 9, .	2.5	27
366	Evolution of bubble microstructure in sheared rhyolite: Formation of a channelâ€ike bubble network. Journal of Geophysical Research, 2008, 113, .	3.3	86
367	Chondrulelike Objects in Short-Period Comet 81P/Wild 2. Science, 2008, 321, 1664-1667.	12.6	215
368	Simultaneous acquisition of dual analyser-based phase contrast X-ray images for small animal imaging. European Journal of Radiology, 2008, 68, S49-S53.	2.6	15
369	Phase contrast X-ray imaging for the non-invasive detection of airway surfaces and lumen characteristics in mouse models of airway disease. European Journal of Radiology, 2008, 68, S22-S26.	2.6	30
370	High-resolution visualization of tumours in rabbit lung using refraction contrast X-ray imaging. European Journal of Radiology, 2008, 68, S54-S57.	2.6	10
371	Origin and formation of iron silicide phases in the aerogel of the Stardust mission. Meteoritics and Planetary Science, 2008, 43, 121-134.	1.6	45
372	Floral Evidence of Annonaceae from the Late Cretaceous of Japan. International Journal of Plant Sciences, 2008, 169, 908-917.	1.3	47
373	X-Ray Microtomographic Imaging of Three-Dimensional Structure of Soft Tissues. Tissue Engineering - Part C: Methods, 2008, 14, 359-363.	2.1	30
374	Dynamic measures of regional lung air volume using phase contrast x-ray imaging. Physics in Medicine and Biology, 2008, 53, 6065-6077.	3.0	83
375	<i>In situ</i> observation of nucleation, fragmentation and microstructure evolution in Sn–Bi and Al–Cu alloys. International Journal of Cast Metals Research, 2008, 21, 125-128.	1.0	48
376	Change in microstructure of Al–Si–Cu casting alloys during high temperature solution treatment. International Journal of Cast Metals Research, 2008, 21, 114-118.	1.0	5
377	Structural Analysis of Filler in Rubber Composite under Stretch with Time-Resolved Two-Dimensional Ultra-Small-Angle X-Ray Scattering. Rubber Chemistry and Technology, 2008, 81, 541-551.	1.2	24
378	Characterization of a Hard X-ray Telescope at Synchrotron Facility SPring-8. Japanese Journal of Applied Physics, 2008, 47, 5743.	1.5	22

#	Article	IF	CITATIONS
379	Direct Observation and Image-Based Simulation of Three-Dimensional Tortuous Crack Evolution inside Opaque Materials. Physical Review Letters, 2008, 100, 115505.	7.8	32
380	Measurement of electron density in dualâ€energy xâ€ray CT with monochromatic x rays and evaluation of its accuracy. Medical Physics, 2008, 35, 4924-4932.	3.0	19
381	Dose distribution of a 125 keV mean energy microplanar x-ray beam for basic studies on microbeam radiotherapy. Medical Physics, 2008, 35, 3252-3258.	3.0	20
382	Thermo-mechanical fatigue property of a surface-hardened AC4CH cast aluminum alloy. Keikinzoku/Journal of Japan Institute of Light Metals, 2008, 58, 236-241.	0.4	1
383	Three-dimensional observation of ductile fracture process by deflection contrast imaging in cast Al–7%Si alloys. Keikinzoku/Journal of Japan Institute of Light Metals, 2008, 58, 58-64.	0.4	6
384	Microfabric analysis of the surficial layer of deep-sea sediments by micro X-ray CT: an example from the Nansei-shoto (Ryukyu) Trench. Journal of the Geological Society of Japan, 2008, 114, III-IV.	0.6	0
385	Microstructural Quantification of Granular Assembly studied by Micro X-ray CT at SPring-8. Journal of Applied Mechanics, 2008, 11, 507-515.	0.1	10
386	3D Particle Characteristics of Highland Lunar Soil (No. 60501) Obtained by Micro X-Ray CT. , 2008, , .		2
387	Facile Synthesis of <i>C</i> ₂ -Symmetric Chiral Crown Ethers with Two Reactive Hydroxymethyl Groups. Synthesis, 2007, 2007, 2973-2978.	2.3	3
388	Imaging lung aeration and lung liquid clearance at birth. FASEB Journal, 2007, 21, 3329-3337.	0.5	177
389	Small airway changes in healthy and ovalbumin-treated mice during quasi-static lung inflation. Respiratory Physiology and Neurobiology, 2007, 156, 304-311.	1.6	20
390	Biphasic change and disuse-mediated regression of canal network structure in cortical bone of growing rats. Bone, 2007, 41, 239-246.	2.9	18
391	Wavelet-based local region-of-interest reconstruction for synchrotron radiation x-ray microtomography. Journal of Applied Physics, 2007, 102, 114908.	2.5	9
392	Characterization of two-dimensional ultra-small-angle X-ray scattering apparatus for application to rubber filled with spherical silica under elongation. Journal of Applied Crystallography, 2007, 40, s397-s401.	4.5	50
393	Computed tomography imaging of the neuronal structure ofDrosophilabrain. Journal of Synchrotron Radiation, 2007, 14, 282-287.	2.4	47
394	Analysis of inner structure in high-strength biodegradable fibers by X-ray microtomography using synchrotron radiation. Polymer, 2007, 48, 6145-6151.	3.8	23
395	Can the changes in sediment concentration be recorded by the three-dimensional grain fabric in plane-bed deposits? :. Journal of the Sedimentological Society of Japan, 2007, 64, 111-115.	0.3	0
396	Formation of Highly Ordered Structure in Poly[(R)-3-hydroxybutyrate-co-(R)-3-hydroxyvalerate] High-Strength Fibers. Macromolecules, 2006, 39, 2940-2946.	4.8	94

#	Article	IF	CITATIONS
397	The Rubble-Pile Asteroid Itokawa as Observed by Hayabusa. Science, 2006, 312, 1330-1334.	12.6	761
398	Comet 81P/Wild 2 Under a Microscope. Science, 2006, 314, 1711-1716.	12.6	848
399	Elemental Compositions of Comet 81P/Wild 2 Samples Collected by Stardust. Science, 2006, 314, 1731-1735.	12.6	200
400	Three-dimensional observation of nanoscopic precipitates in an aluminum alloy by microtomography with Fresnel zone plate optics. Applied Physics Letters, 2006, 89, 143112.	3.3	49
401	Microbeam X-ray Diffraction and Enzymatic Degradation of Poly[(R)-3-hydroxybutyrate] Fibers with Two Kinds of Molecular Conformations. Macromolecules, 2006, 39, 5789-5795.	4.8	78
402	Monochromatic synchrotron radiation μCT reveals disuse-mediated canal network rarefaction in cortical bone of growing rat tibiae. Journal of Applied Physiology, 2006, 100, 274-280.	2.5	43
403	Development of micro-tomography system with Fresnel zone plate optics at SPring-8. , 2006, , .		35
404	2P369 Microtomographic analysis of Drosophila brain(44. Neuro-biophysics,Poster) Tj ETQq0 0 0 rgBT /Overlock	10 Tf 50 4	62 Td (Sessio
405	Fast tomography using quasi-monochromatic undulator radiation. Journal of Synchrotron Radiation, 2006, 13, 403-407.	2.4	23
406	New approaches to fabrication of multilayer Fresnel zone plate for high-energy synchrotron radiation X-rays. Vacuum, 2006, 80, 823-827.	3.5	19
407	Quantitative assessment of microstructure and its effects on compression behavior of aluminum foams via high-resolution synchrotron X-ray tomography. Metallurgical and Materials Transactions A: Physical Metallurgy and Materials Science, 2006, 37, 1211-1219.	2.2	93
408	3-D Image-Based Mechanical Simulation of Aluminium Foams: Effects of Internal Microstructure. Advanced Engineering Materials, 2006, 8, 459-467.	3.5	26
409	In-situ High-resolution X-ray CT Observation of Compressive and Damage Behaviour of Aluminium Foams by Local Tomography Technique. Advanced Engineering Materials, 2006, 8, 473-475.	3.5	30
410	Preferential penetration path of gallium into grain boundary in practical aluminium alloy. Philosophical Magazine, 2006, 86, 4351-4366.	1.6	36
411	Fabrication of Porous Aluminium and Copper Media by Using Monotectic Solidification under a Magnetic Field. Materials Science Forum, 2006, 512, 289-294.	0.3	Ο
412	698. Towards Non-Invasive Assessment of CF Airway Gene Therapy: High Resolution Propogation-Based Imaging of Airway Surface Liquid Via Synchrotron Light. Molecular Therapy, 2006, 13, S270.	8.2	0
413	Nondestructive Evaluation of Thermal Phase Growth in Solder Ball Micro-Joints by Synchrotron Radiation X-Ray Micro-Tomography. , 2005, , 1115.		4
414	Three-dimensional observation of the entangled eutectic structure in the Al2O3–YAG system. Journal of the European Ceramic Society, 2005, 25, 1397-1403.	5.7	22

#	Article	IF	CITATIONS
415	Unification of analyser-based and propagation-based X-ray phase-contrast imaging. Nuclear Instruments and Methods in Physics Research, Section A: Accelerators, Spectrometers, Detectors and Associated Equipment, 2005, 548, 163-168.	1.6	17
416	Phase contrast X-ray imaging of mice and rabbit lungs: a comparative study. British Journal of Radiology, 2005, 78, 1018-1027.	2.2	81
417	Structure investigation of narrow banded spherulites in polyhydroxyalkanoates by microbeam X-ray diffraction with synchrotron radiation. Polymer, 2005, 46, 5673-5679.	3.8	43
418	Morphometric Deformations of Small Airways and Alveoli under Quasi-static Inflation Process. Journal of Physiological Anthropology and Applied Human Science, 2005, 24, 465-468.	0.4	6
419	Dynamic imaging of the lungs using x-ray phase contrast. Physics in Medicine and Biology, 2005, 50, 5031-5040.	3.0	104
420	Application of synchrotron x-ray microtomography to investigate ductile fracture in Al alloys. Applied Physics Letters, 2005, 87, 241907.	3.3	46
421	Quantitative evaluation of attenuation contrast of X-ray computed tomography images using monochromatized beams. American Mineralogist, 2005, 90, 132-142.	1.9	61
422	Refraction-enhanced tomography of mouse and rabbit lungs. Medical Physics, 2005, 32, 2787-2792.	3.0	30
423	Localized morphometric deformations of small airways and alveoli in intact mouse lungs under quasi-static inflation. Respiratory Physiology and Neurobiology, 2005, 147, 51-63.	1.6	21
424	Construction and Commissioning of A 248 m-long Beamline with X-ray Undulator Light Source. AIP Conference Proceedings, 2004, , .	0.4	64
425	Direct Measurement of the Resolving Power of X-ray CT System in SPring-8. AIP Conference Proceedings, 2004, , .	0.4	9
426	X-ray imaging microscopy using Fresnel zone plate objective and quasimonochromatic undulator radiation. Review of Scientific Instruments, 2004, 75, 1155-1157.	1.3	9
427	Three-dimensional diffusion of non-sorbing species in porous sandstone: computer simulation based on X-ray microtomography using synchrotron radiation. Journal of Contaminant Hydrology, 2004, 74, 253-264.	3.3	58
428	On the origin of speckle in x-ray phase contrast images of lung tissue. Physics in Medicine and Biology, 2004, 49, 4335-4348.	3.0	129
429	A large-area CMOS imager as an X-ray detector for synchrotron radiation experiments. Journal of Synchrotron Radiation, 2004, 11, 347-352.	2.4	21
430	Processing of a Strong Biodegradable Poly[(R)-3-hydroxybutyrate] Fiber and a New Fiber Structure Revealed by Micro-Beam X-Ray Diffraction with Synchrotron Radiation. Macromolecular Rapid Communications, 2004, 25, 1100-1104.	3.9	111
431	Novel application of sputtered-sliced concentric multilayers to various optical elements for synchrotron radiation high-brilliance X-ray beamlines at SPring-8. Vacuum, 2004, 74, 741-746.	3.5	2
432	Fabrication of porous aluminum with deep pores by using Al–In monotectic solidification and electrochemical etching. Materials Letters, 2004, 58, 911-915.	2.6	31

#	Article	IF	CITATIONS
433	Experimental reproduction of classic barred olivine chondrules: open-system behavior of chondrule formation. Geochimica Et Cosmochimica Acta, 2004, 68, 653-672.	3.9	22
434	Nondestructive three-dimensional element-concentration mapping of a Cs-doped partially molten granite by X-ray computed tomography using synchrotron radiation. American Mineralogist, 2004, 89, 1304-1313.	1.9	35
435	Bone structure and mineralization demonstrated using synchrotron radiation computed tomography (SR-CT) in animal models: preliminary findings. Journal of Bone and Mineral Metabolism, 2003, 21, 287-293.	2.7	46
436	Electron density measurement with dual-energy x-ray CT using synchrotron radiation. Physics in Medicine and Biology, 2003, 48, 673-685.	3.0	122
437	Distribution of electron density using dual-energy X-ray CT. IEEE Transactions on Nuclear Science, 2003, 50, 1678-1682.	2.0	9
438	Direct Three-Dimensional Observation of Phase Structures in a Non-aqueous Physical Gel by Synchrotron X-ray CT. Kobunshi Ronbunshu, 2003, 60, 373-376.	0.2	3
439	Observations of three-dimensional microstructures of symplectite minerals in the Horoman Peridotite Complex using a high-resolution X-ray CT system at Spring-8. Journal of the Geological Society of Japan, 2003, 109, III-IV.	0.6	7
440	High-sensitive imaging with scanning transmission hard X-ray microscope. European Physical Journal Special Topics, 2003, 104, 41-44.	0.2	13
441	Application of Concentric Multilayers to Various X-ray Optical System. Shinku/Journal of the Vacuum Society of Japan, 2003, 46, 261-264.	0.2	1
442	Submicrometer-resolution three-dimensional imaging with hard x-ray imaging microtomography. Review of Scientific Instruments, 2002, 73, 4246-4249.	1.3	50
443	X-ray refraction-enhanced imaging and a method for phase retrieval for a simple object. Journal of Synchrotron Radiation, 2002, 9, 160-165.	2.4	80
444	Development of high spatial resolution X-ray CT system at BL47XU in SPring-8. Nuclear Instruments and Methods in Physics Research, Section A: Accelerators, Spectrometers, Detectors and Associated Equipment, 2001, 467-468, 853-856.	1.6	85
445	Micro- and macrobehavior of granitic rock: observations and viscoelastic homogenization analysis. Computer Methods in Applied Mechanics and Engineering, 2001, 191, 47-72.	6.6	38
446	Hard X-Ray Microtomography Using X-Ray Imaging Optics. Japanese Journal of Applied Physics, 2001, 40, 1499-1503.	1.5	11
447	<title>X-ray imaging microscope with a partial coherent illumination</title> ., 2001, , .		5
448	SPring-8ā«āŠāʿā,‹é«~å^†è§£èƒ½Xç-šCTè£ç½® (XTM) ā®é–‹ç™ºã¨āā®éš•石ā,ā®å¿œç"". Ganseki Kobutsu Ka	gaku,@ 0 01,	30194-95.

449	A Study of Three-dimensional Structures of Rocks and Minerals Using a High-resolution X-ray CT Method. Journal of Geography (Chigaku Zasshi), 2000, 109, 845-858.	0.3	7

450 <title>Development of microtomography imaging system for rock and mineral samples</title>., 1999, 3772, 214.

#	Article	IF	CITATIONS
451	3D/4D Strain Mapping Using <i>In Situ</i> X-Ray Microtomography. Applied Mechanics and Materials, 0, 70, 249-254.	0.2	1
452	<i>In Situ</i> Study of the Altering Globule Packing-Density during Semisolid Alloy Deformation. Solid State Phenomena, 0, 192-193, 185-190.	0.3	0
453	Assessment of Deformation Behavior of Polycrystalline Aluminum Using Diffraction-Amalgamated Grain-Boundary Tracking (DAGT) Technique. Materials Science Forum, 0, 794-796, 57-62.	0.3	Ο
454	Dichotomy in formation and growth of bones of Yanornis martini (Pygostylia, Ornithuromorpha): study of thermal regime in an extinct bird. Historical Biology, 0, , 1-24.	1.4	2